Charge order in the Pr substituted $YBa_2Cu_3O_7$ from high-field Hall effect measurements

C. M. Duffy[1,†], M. Altangerel[1,2,3], S. Badoux[1], D. Vignolles[1,3], T. Oustric[2], C. M. Moir[4], Keke Feng[4], A. Frano[4], M. B. Maple[4], L. Taillefer[2,3,5] and C. Proust[1,3,‡]

[1] *Univ. Toulouse, INSA-T, Univ. Grenoble Alpes, CNRS, LNCMI-EMFL, UPR3228, Toulouse, France.*

[2] *Institut quantique, Département de physique & RQMP, Université de Sherbrooke, Sherbrooke, Québec, Canada*

[3] *Université de Sherbrooke–CNRS and IRL Frontières Quantiques, Sherbrooke, Québec, Canada.*

[4] *Department of Physics, Center for Advanced Nanoscience, University of California, San Diego, CA 92093, USA.*

[5] *Canadian Institute for Advanced Research, Toronto, Ontario M5G 1M1, Canada*

(Dated: March 30, 2026)

The mechanism of doping in the composite $Pr_xY_{1-x}Ba_2Cu_3O_{7-\delta}$ (Pr-YBCO) system is distinct from that of pure YBCO, offering a means to explore the requirements for the numerous electronic orders appearing in the phase diagram. One such example is the ubiquitous 2D charge order and concomitant Fermi surface reconstruction in underdoped YBCO. Here, using Hall effect measurements, we find signatures of a Fermi surface reconstruction similar to that in pure YBCO indicating the presence of 2D charge order in Pr-YBCO. Additionally, we find that the phase diagrams of Pr-YBCO and YBCO are symmetric despite the additional disorder in the former and the distinction between hole depletion through Pr substitution and through O reduction. This indicates that while the mechanism of doping differs, the amount of charge carriers in the planes is the most important factor governing the electronic orders in these systems.

I. INTRODUCTION

The discovery of $YBa_2Cu_3O_{7-\delta}$ (YBCO) marked a paradigm shift in the field of high-T_c superconductivity. Its high maximum T_c at optimal doping (90 K), cleanliness, and ease of synthesis have made it a key system for studies on high-T_c cuprates. The complete chemical substitution of Y for any rare-earth element (such as Nd, Er, and Gd) has no impact on T_c with a few exceptions: Ce and Tb which do not readily form the orthorhombic crystal structure of YBCO, Pm which is radioactively unstable, and Pr which forms a stable, isostructural system with the caveat of being an insulator [1]. The composite system $Pr_xY_{1-x}Ba_2Cu_3O_{7-\delta}$ (Pr-YBCO), whose phase diagram is presented in Fig. 1, demarcates the superconducting and insulating states, offering a unique insight into the role of doping, disorder, and oxygen in the YBCO system. Superconductivity is continually tuned through Pr cation substitution while retaining the oxygen stoichiometry, with the suppression of superconductivity at $x > 0.55$ and a metal-insulator crossover leading to a fully insulating phase when $x = 1$ [1–4].

The effects of Pr substitution are multifaceted. The conduction electrons of Pr originate from $4f$ orbitals and in its trivalent form (the dominant form in Pr-YBCO [3, 4]) the ionic radius of Pr is larger than that of Y. This directly disturbs the adjacent CuO_2 planes, essential for superconductivity. Rather than altering the chain stoichiometry by a reduction of oxygen, the chains in Pr-YBCO are largely unaffected by Pr doping [5]. Instead, hole doping in the planes is varied through two distinct mechanisms: orbital hybridization between the Pr$4f$ and O$2p$ orbitals in the CuO_2 plane leading to hole localization [6], and pair breaking due to the enhanced disorder in particular via a spin exchange interaction between the holes and the magnetic moment of Pr ions [2]. Recent ARPES measurements in Pr-YBCO challenge this point of view and suggest that the reduction of T_c is due to the donation of electrons to the CuO_2 planes [7].

Considering these dissimilarities between the structure and doping of YBCO and Pr-YBCO, it is perhaps unexpected that the phase diagram of Pr-YBCO in Fig. 1 resembles closely that of pure YBCO [8] comprising antiferromagnetic and superconducting domes with similar dependencies on their respective doping. Muon spin-relaxation and NMR have tracked the termination of AFM order from the Pr spins to $x = 0.4$ [9, 10] which lies within the superconducting dome. Similarly, AFM order within the SC dome has been detected by neutron spectroscopy in YBCO [11].

One crucial observation that has recently been reported in Pr-YBCO [12, 13] is the existence of short-range charge order which appears universal in the phase diagram of underdoped cuprates and intertwines strongly with SC and magnetic order [14–23]. In YBCO, charge order manifests as a plateau in the superconducting dome centred around a doping of $\frac{1}{8}$ [24–27]. Near this doping level there is a depression of the upper critical field H_{c2} [28] and an enhancement of T_c under the applica-

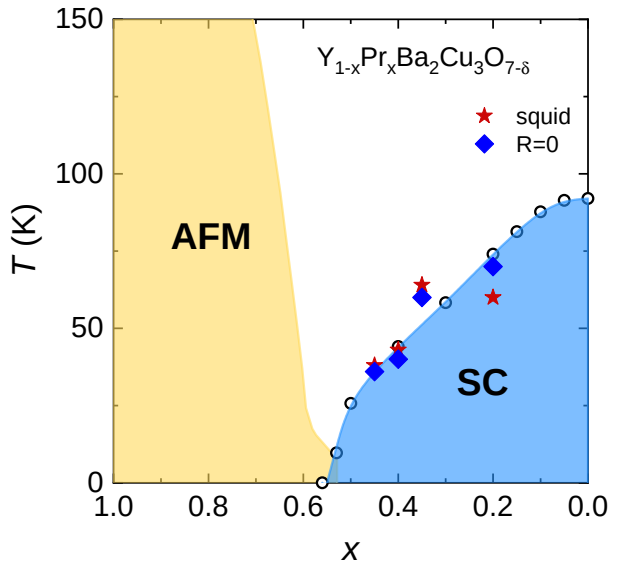

FIG. 1. The phase diagram of Pr-YBCO. The yellow region marks the antiferromagnetic (AFM) region bounded by T_N. Muon spin-relaxation measurements reveal two types of magnetic order: the suppression of the Mott state, and magnetic order from the Pr spin. Black circles are T_c versus nominal Pr content x from ref. [5]. The superconducting dome is marked in blue. The star (diamond) symbols correspond to T_c measured by squid (resistivity) in the four Pr-YBCO samples presented in this study.

tion of hydrostatic pressure [29] providing clear evidence for competition between SC and charge order. In underdoped YBCO and Hg-based cuprates, the change of the dominant carrier type is demarcated by a sign reversal in the low-T Hall effect [8, 20, 30, 31] and in the Seebeck coefficient [32, 33]. The negative sign of both quantities observed at low doping levels is consistent with a Fermi surface containing at least a mobile electron pocket. The doping range over which this sign change appears [8, 30] is roughly consistent with the regime in which NMR and x-ray measurements find a high-T biaxial charge order in the CuO_2 planes, although it has been noted recently that the endpoint of CDW order as a function of hole is not easy to define [34]. Quantum oscillation measurements in underdoped YBCO [35–37] and Hg-based cuprates [20, 38, 39] have shown a low frequency oscillation alluding to a Fermi surface comprising small pockets. This is in stark contrast to overdoped Tl2201 which hosts a large hole-like Fermi surface [40], as predicted by band structure calculations. Supporting theoretical investigations have found that the reconstruction of the large Fermi surface into small electron-like pockets is consistent with a Fermi surface reconstruction (FSR) by biaxial charge order [20, 41]. This biaxial charge order is short ranged with a correlation length up to 60 Å and has half integer out of plane modulation. The wavevectors characterizing charge ordering in YBCO are incommensurate and slightly different along the a- and b-axes.

Under the application of high magnetic fields [42, 43], uniaxial strain [44] and in thin film form [45], YBCO forms coherent 3D charge order which coexists with, and has the same incommensurate ordering vector and doping dependence as the 2D charge order. It has integer out of plane modulation. Measurements on detwinned crystals have shown that the 3D charge order modulations are uniaxial along the b-axis. The maximum achieved in-plane correlation length is about 200 Å at $B = 28$ T [46].

In Pr-YBCO, signatures of 3D charge order were found using resonant x-ray scattering (REXS) at $x = 0.3$ ($T_c = 50$ K) [47]. These signatures were only observed at integer out of plane (L) modulation with a correlation length exceeding 360 Å and no indication of the biaxial 2D charge order at half-integer values of L. The intensity of the peak associated with the 3D charge order was detectable at room temperature and grew with temperature, reaching a maximum at T_c, similar to pure YBCO [48]. This was interpreted as a strong indication that 3D charge order in Pr-YBCO was stabilized by the extended dimensionality of the Pr4f orbitals. A subsequent study [12] using soft REXS on thin films of Pr-YBCO across the entire doping series found two charge order peaks at half-integer L suggesting 2D charge order similar to pure YBCO, but not at integer L e.g. without the stabilized 3D charge order. More recently, a study combining grazing incidence x-ray diffraction and REXS measurements on thin films of Pr-YBCO at $x = 0.3$ found two distinct charge orders with similar in-plane periodicity but with different value of L [13]. The peak at L=1 (attributed to 3D charge order in ref. [47]) was interpreted as a Pr-related super-lattice structure, while the peak at L=0.5 was interpreted as evidence of biaxial 2D charge order. The 2D charge correlations were found at high temperatures with a short correlation length of $25 - 30$ Å – 3 times smaller than that of pure YBCO [49]. Despite the discrepancies reported by different groups in Pr-YBCO, there is clear evidence of charge modulations in this system.

It is not obvious whether these short-range correlations would suffice to reconstruct the Fermi surface in Pr-YBCO. To probe this, we have performed Hall effect measurements on twinned Pr-YBCO crystals spanning the doping range $x = 0.2 - 0.45$ and $T_c = 42 - 65$ K. We find a T-dependent sign-change in R_H which disappears with increasing Pr content (decreasing T_c) and is reminiscent of that in YBCO, indicating the presence of a density wave order and a concomitant Fermi surface reconstruction. We propose that this density wave order stems from charge correlations and that the apparent lack of competition with superconductivity is a consequence of the short correlation length [12] in addition to high disorder levels. The doping level at which the reconstruction terminates coincides with the onset of the metal-insulator crossover from Pr spin at $x = 0.4$ [9], highlighting the complex relationship between magnetic and charge order. Overall, we find stark similarities between the phase diagrams of Pr-YBCO and YBCO, and

discuss the results in the context of disorder and the disparate mechanisms of doping holes into the CuO_2 planes.

II. EXPERIMENTAL METHODS

Crystals of Pr-YBCO were synthesised in UC San Diego according to the method described in ref. [50] using a solid-state reaction to generate the precursor material which was added to a flux, composed of $BaCO_3$ and CuO. Precursor and flux were slowly brought up to a temperature of 900 °C and held for 1 hour. Then, the temperature was decreased to 880 °C to allow crystals to form, before the temperature was reduced slowly to room temperature. The crystals were then annealed in gold coated quartz trays at 400 °C for 5 days in oxygen and allowed to cool naturally to room temperature. The crystals were then characterised using SQUID magnetometry. Gold contacts were sputtered onto both faces of polished crystals and annealed at 400°C for two hours in flowing oxygen to allow the gold to diffuse. Electrical contacts were made using DuPont 4929N. The typical sample dimensions were on the order of $\sim 200 - 600$ μm in length and breadth, and $30 - 100$ μm in thickness. Pulsed magnetic field measurements up to 65 T were carried out at He-4 temperatures at the LNCMI-EMFL in Toulouse with two field polarities at each temperature to allow for a standard symmetrization and antisymmetrization of the magnetoresistance and Hall resistance, respectively. Note that c-axis contamination was observed in the resistivity ρ_{xx} measurements but does not alter the Hall measurements due to the antisymmetrization. The six crystals, their nominal Pr content, and their T_c from SQUID (defined at the onset, see Appendix A) and dc resistivity (defined where $R = 0$, see Appendix A) are shown in Table I; the discrepancies between the two values are discussed below. The dimensions of the samples are shown in Appendix B. To isolate the effect of Pr only, the chains were fully loaded with oxygen ($y = 7$). Small deviations from optimal oxygen doping are possible, but are not responsible for the results reported herein. Due to the complex relation between Pr- and hole-doping and our inability to determine both the precise oxygen content and precise Pr content, it is not possible to label our samples with a specific hole doping p. We therefore use T_c as a measure of sample doping and to facilitate comparison with YBCO.

III. RESULTS

The Hall coefficient $R_H(T)$ measured at the maximum field strength of four representative samples of Pr-YBCO is shown as a function of temperature in Fig. 2. The raw data R_H versus magnetic field for the four samples are shown in Appendix C. The duplicates of $x = 0.35$ and $x = 0.45$ gave the same results as those shown (see Appendix D) and are not included in the figures for clarity.

Sample	Nominal Pr x	T_c^{SQUID} (K)	T_c^{res} (K)
0.2	0.2	60	70
0.35a	0.35	64	61
0.35b	0.35	65	57
0.4	0.4	43	37
0.45a	0.45	38	32
0.45b	0.45	42	35

TABLE I. Samples measured in this work with their nominal Pr content and transition temperature measured by SQUID and by resistivity. The discrepancy between the T_c values is a possible consequence of inherent disorder and inhomogeneity in the system.

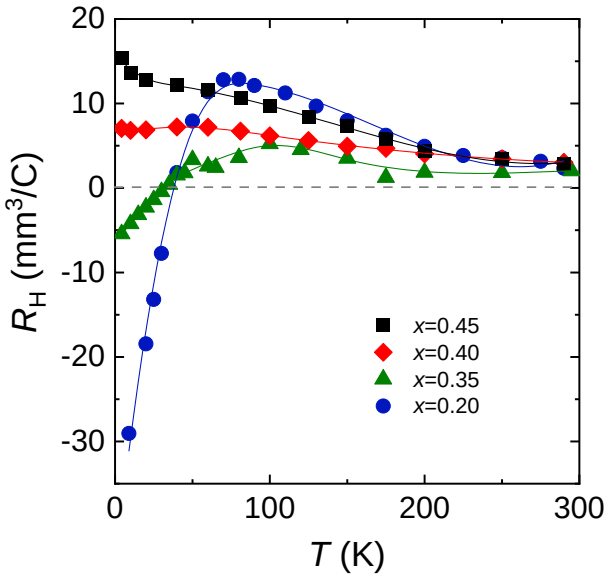

FIG. 2. $R_H(T)$ for four samples showing a change of sign at higher T_c. The temperature at which this occurs (T_0) decreases in parallel with T_c, eventually remaining positive for the low-T_c crystals. The same behaviour is observed in the two samples which are not shown.

At high temperature where the Hall effect is perfectly linear in-field, we perform measurements up to 30 T and a linear extrapolation of R_H up to 65 T is used. In all samples, $R_H(T)$ grows with decreasing T; below $T = 100$ K, the different doping levels exhibit distinct behaviour. In the samples with the higher Pr content (lower T_c) R_H grows with temperature and shows an upturn at low temperatures. In contrast, the samples with a lower Pr content (higher T_c) reach a maximum in $R_H(T)$ before sharply falling and changing sign, hence suggesting a FSR occurring in the doping phase diagram of Pr-YBCO outwith the region where the metal-insulator crossover occurs. T_0, the temperature at which $R_H = 0$, decreases with increased Pr doping (decreasing T_c). This is our first main finding: the Hall coefficient of Pr-YBCO with varying x mirrors the behaviour of pure YBCO with varying p.

IV. COMPARISON WITH YBCO

To emphasize this point, in Fig. 3, we plot R_H versus magnetic field at T=10 K for (a) Pr-YBCO and (b) YBCO (from ref. [30]). The same general trends are evident in the two materials - at higher T_c, R_H is negative whereas closer to the Mott state it is positive. As a reminder, in YBCO, the positive Hall effect at low doping ($p < 0.08$) has been interpreted as a consequence of a FSR by an antiferromagnetic order. In this scenario, the FS consists of two hole pockets in the first Brillouin zone. This is in agreement with ARPES and QO studies showing the metallic character of the AFM phase at low doping in the IPs of a 5-layer cuprate [51]. At higher doping ($0.08 < p < 0.16$), the FS is reconstructed by charge order, presumably biaxial, which gives rise to an electron pocket and a negative Hall effect. In Pr-YBCO, the same phenomenology applies since for lower T_c, the Hall effect remains positive at $T = 10$ K. This is justified by evidence for antiferromagnetic ordering of the Pr moments and the Cu moments within the Cu-O planes for $x > 0.4$ by μSR and NMR measurements [9, 10]. For the higher T_c samples, the Hall effect changes sign at low temperature.

In Fig. 4, we compare the temperature dependence of R_H normalized by its value at $T = 100$ K and measured at high fields for several dopings of (a) Pr-YBCO and (b) YBCO (from ref. [30]). Again, the similarity is striking. In YBCO, $R_H(T)$ goes from positive at $T = 100$ K to negative as $T \to 0$, except for $p = 0.078$, where $R_H(T)$ never changes sign and increases monotonically with decreasing temperature. In Pr-YBCO, $R_H(T)$ goes from positive at $T = 100$ K to negative as T $\to 0$ for $x = 0.2$ and $x = 0.35$, but never changes sign for $x = 0.4$ and $x = 0.45$. The sign reversal of the Hall effect is a signature of the presence of charge order and of an electron pocket in the reconstructed FS.

One notable dissimilarity between the two materials is the doping-dependence of the upper critical field, H_{c2}, defined as the irreversibility field at $T = 0$, $H_{irr}(T \to 0)$. This is shown in Fig. 5 and the determination of H_{c2} for Pr-YBCO is discussed in Appendix E. In the Pr-YBCO system, an increase of Pr leads to a monotonic quenching of H_{irr}. The situation is more complicated in YBCO where H_{irr} shows a clear suppression with increased hole doping, reaching a minimum near $p = 0.125$ before increasing again towards p^* [28, 30]. The apparent lack of competition in Pr-YBCO in the zero-field resistivity [1, 5] and the critical field [52], shown in Fig. 5, poses a challenge to the reconstruction of the FS due to 2D charge order - if charge correlations do not compete measurably with superconductivity, are they able to cause a FSR? This hence leads to our second finding: the competition between superconductivity and 2D charge order in Pr-YBCO appears less pronounced than in YBCO.

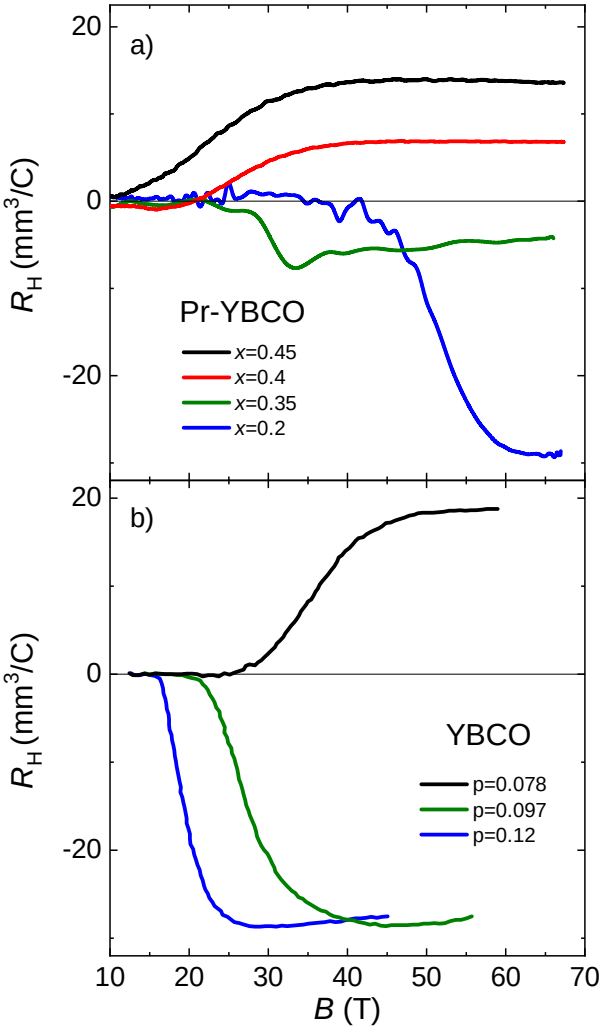

FIG. 3. (a) R_H as a function of magnetic field at $T = 10$ K showing quite clearly the sign change that occurs and its doping dependence in Pr-YBCO. (b) The same plot but for pure YBCO at several doping levels (from ref. [30]).

V. DISCUSSION

1. *Doping mechanism*

The substitution of Pr for Y is accompanied by subtle changes to the unit cell and a hybridisation between Pr4f orbitals and O2p orbitals, both of which affect the electronic character of Pr-YBCO. The larger ionic radius of Pr and its magnetic moment act as a source of disorder provoking a direct effect of Pr on the CuO_2 planes, hence on superconductivity and charge order.
Superconductivity in the cuprates is governed by the charge carriers in the CuO_2 planes. In pure YBCO the hole doping within the planes is governed by the oxygen stoichiometry of the CuO chains which act as charge reservoirs. In Pr-YBCO, the dominant Pr ion (Pr^{3+}) localizes carriers in the CuO_2 planes as a consequence of

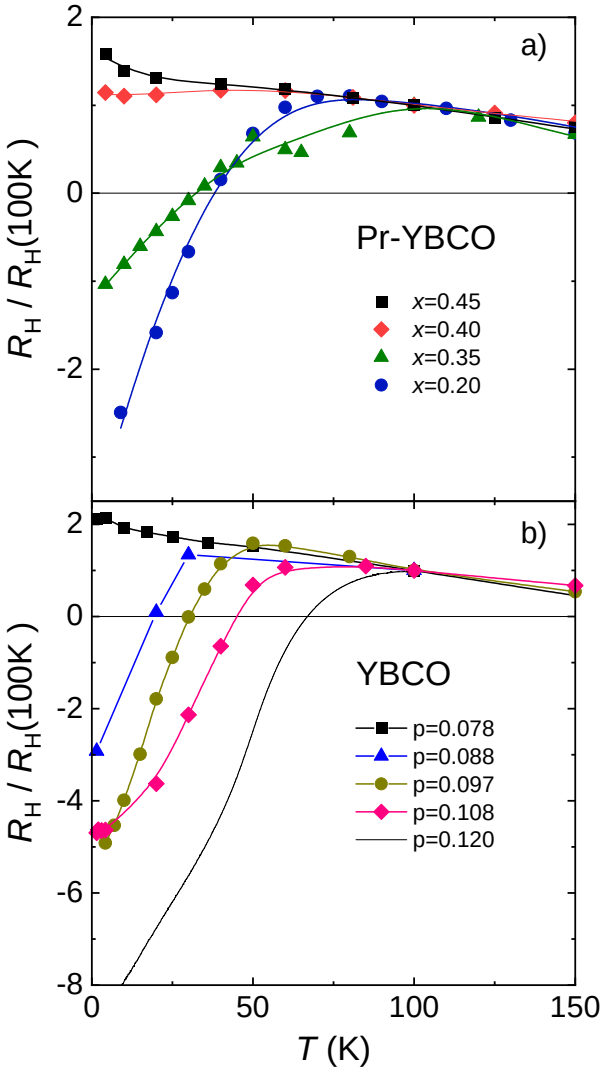

FIG. 4. $R_H(T)$ normalized by its value at $T = 100$ K for (a) Pr-YBCO (this work) and (b) YBCO (from ref. [30]). Both show a systematic variation of T_0 with doping while the doping levels closest to the antiferromagnetic phase does not exhibit a sign change.

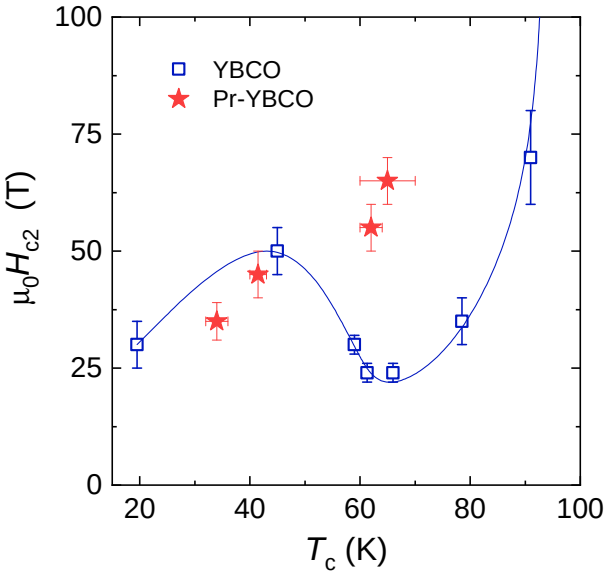

FIG. 5. H_{c2} for YBCO [28] (blue squares) and Pr-YBCO (red stars) as a function of T_c. The clear depression seen in YBCO is not observed in Pr-YBCO representing the weaker competition between charge correlations and superconductivity in the latter. A monotonic dependence of H_{c2} in Pr-YBCO has also been observed in a more extensive doping range in ref. [52] (see Appendix E for a discusssion)

orbital hybridization [6], but this interpretation has been challenged recently [7]. In the case of the former, the localized holes no longer contribute to the transport or superconducting properties and thus T_c gradually falls with increased Pr content in the same way as T_c falls as the CuO chains are diminished of oxygen. The depletion of superconductivity is further supplemented by pair-breaking effects due to disorder from the Pr. Note that none of the mechanisms which suppress superconductivity involve a change of the oxygen ordering in the CuO chains, and hence are entirely distinct from doping in YBCO. Nonetheless, in both YBCO and Pr-YBCO, the in-plane hole concentration is dictated by an out-of-plane influence and hence it is not unusual that the electronic behaviour associated with the planes be near analogous in the two systems.

2. *Fermi surface reconstruction*

On a similar vein, it is not unexpected that 2D charge order and a FSR are both present in Pr-YBCO, in particular, considering their universality in the cuprates [8, 20, 32, 39]. Grazing incidence x-ray diffraction and REXS measurements on thin films of Pr-YBCO found charge order peaks at half-integer L which have been interpreted as signatures of 2D charge order similar to YBCO [12, 13]. Furthermore, it is natural to conclude by comparison that the FSR reported here is a consequence of such 2D charge order. Although the correlation length is 3 times smaller than that of YBCO, we cannot exclude that it increases under a strong magnetic field, as it is the case in YBCO [42, 46].

Unique to YBCO are uniaxial 3D charge correlations along the b-axis which appear under external influences such as stress [44, 48], in thin films [45], and in magnetic fields exceeding 15 T [42, 43, 53]. The 3D charge order is superimposed on the 2D charge order, sharing the same incommensurate wave vector. The out-of-plane coherence is mediated by phase-locking of the CuO_2 bilayers. The in-plane correlation length can be as high as 200 Å at $B = 30$ T, compared to 80-100 Å for the 2D charge order.

The exact mechanism of the FSR in YBCO by the CDW is still debated. Biaxial charge order with wavevectors

$(Q_x, 0)$ and $(0, Q_y)$ creates a small electron-like pocket located at the nodes. This is the most natural scenario for the FSR, although it has been argued that the value of the coherence length of $YBa_2Cu_3O_{6.59}$ is too short to be at the origin of quantum oscillations at this doping level [54]. The 3D charge order has a longer coherence length but is uniaxial. Unidirectional charge order can create an electron-like pocket but only in the presence of nematic order and it would be located at the antinodes, where the pseudogap removes the density of states [55]. There are other arguments against the scenario of FSR by 3D charge order. Since the incommensurate wave vector is identical to the one of the 2D charge order, it does not introduce a new periodicity. Although the onset of the 3D charge order is closer to the temperature at which R_H changes sign, T_0, it was pointed out that for $p > 0.12$, T_0 is larger than the onset of 3D charge order hence it is largely inert with respect to the FSR [53]. This conclusion was also inferred from a transport study under uniaxial strain where the impact of 3D charge order was argued to be too weak to explain the sign reversal of the Hall coefficient as a function of temperature [56]. A recent REXS study on YBCO has shown that the stress induced 3D charge order is observed only in $y = 6.5$ and $y = 6.67$, while the sign reversal of the Hall effect occurs at least in the doping range between $y = 6.48$ and $y = 6.86$.

It is not clear that Pr-YBCO hosts 3D charge order. The observation of signatures in REXS was supported by the argument that the 3D character of the hybridized Pr4f-O2p orbital could facilitate long-range, out-of-plane charge order [47]. However, a more recent study argued that the signature detected at $x = 0.3$ is due to a superlattice structure given by the 1/3 partial substitution of Pr [13]. More work is needed to elucidate the nature of the 3D charge order in Pr-YBCO, in particular it would be interesting to perform x-ray scattering under magnetic field or uniaxial stress.

3. *Effect of disorder*

In archetypal CDW systems, the effect of disorder is to suppress and to smear the CDW transition. From a theoretical point of view, weak disorder prevents long-range incommensurate CDW order [57]. But the signature of the ideal CDW may still appear in the presence of disorder. This has been demonstrated in Pd-intercalated $ErTe_3$, where two incommensurate CDW phases are progressively suppressed, as the amount of Pd increases [58].

By analogy, we can understand why, for the same T_c, the sign reversal of the Hall effect occurs at lower temperature in Pr-YBCO compared to pure YBCO. This is shown in Fig. 6 where the temperature of the sign reversal of the Hall effect of YBCO (open diamonds) is compared to Pr-YBCO (red stars). Moreover, it is clear that the substitution of Pr results in a threefold decrease of the charge order correlation length [12, 45, 49]. This is also

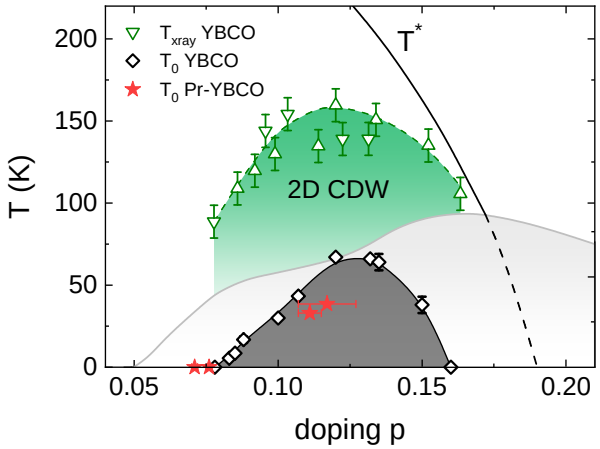

FIG. 6. Comparison of the temperature of the sign reversal of the Hall effect, T_0 of YBCO (open diamonds) and of Pr-YBCO (red stars). The green region marks the 2D charge order detected by x-ray measurements in YBCO (green triangles from refs. [49, 61]). The superconducting dome is marked in gray. The solid black line and its extrapolation (dashed line) represent the pseudogap temperature in YBCO.

the case in Zn-doped YBCO, where Cu in the planes is substituted for Zn impurities, introducing point-like disorder. Similar to Pr-YBCO, T_c is suppressed, with greater suppression at higher Zn percentages; but unlike Pr-YBCO, the decrease of T_c is a direct consequence of pair-breaking and the doping is not modified by Zn substitution. Zn-YBCO hosts definitive charge correlations [59] and measurements (at $B = 14$ T for Zn-YBCO) reveal a sign reversal of the Hall effect at a temperature T_0 which is lower than pure YBCO, depending on the impurity level [60]. Zn doping does not modify the charge order wavevector, but has a drastic effect on the correlation length and intensity; this was argued to be a consequence of suppressed charge correlations around the Zn impurities [59].

4. *Competition between CO and SC*

A direct comparison with YBCO combined with the arguments presented above for Zn-YBCO suggests that 2D charge order in Pr-YBCO causes the FSR seen in Hall measurements. However, there is a lack of evidence in the data for the canonical competition between superconductivity and charge order, traditionally seen as a suppression of T_c and H_{c2} in transport measurements near $p \sim 0.125$. The same effect is observed in Zn-substituted YBCO, where the dip in T_c near p ≈ 0.12 seems to vanish as the Zn content increases [62]. It is pertinent to note that the reduced correlation length in Pr-YBCO alone cannot account for the lack of competition between charge order and superconductivity. Indeed, in the clean single layer cuprate Hg1201, charge order has been reported with a similar correlation length as Pr-YBCO (7-8

lattice spacings) [19] and yet a clear depression of T_c remains manifest [63]. Additionally, quantum oscillations find a single reconstructed pocket in Hg1201, signalling that the correlation length grows at high magnetic field and suffices to reconstruct the FS [38, 39].

If we assume that the correlation length grows at high magnetic field in order to reconstruct the FS, the concealed competition in Pr-YBCO is then also an effect of disorder. The disparate T_c values of our samples raise the question of doping and/or Pr-substitution inhomogeneity. The suppression of the charge order and of SC in Pr-YBCO may not have comparable linear effects. Early pressure studies of the resistivity of Pr-YBCO up to 20 kbar do reveal an enhancement of dT_c/dP in the doping region where we observe a sign change in R_H [64]. Similar results up to 2.5 GPa in YBCO have been interpreted as evidence for the enhancement of superconductivity once the charge order is suppressed by pressure [29]. The enhancement in Pr-YBCO is a factor of ~ 2 smaller than in YBCO at the doping level where charge correlations are expected to be maximal. Additionally, above $P = 6$ kbar, dT_c/dP decreases at $x = 0.3$ hinting that Pr hybridization has a complex effect on competing orders [64].

VI. SUMMARY

Measurements of the Hall coefficient in Pr-YBCO at magnetic fields up to 65 T find that R_H becomes negative in certain doping levels at low temperatures with the temperature at which the sign change occurs, T_0, diminishing with increased Pr doping (decreased T_c). R_H remains positive at all temperatures at high x where the normal state resistivity shows a metal-insulator crossover once superconductivity is suppressed. By analogy with other underdoped cuprates, we attribute the sign change of the Hall effect to a FSR from a large FS to small electron pockets due to 2D charge order.

Despite the differences in disorder and means of doping, the phase diagram of Pr-YBCO is qualitatively similar to pure YBCO. We speculate that this stems from the fact that the charge carriers within the planes are controlled by an out-of-plane influence in both systems: the CuO chain charge reservoirs in YBCO, and hole localisation in Pr-YBCO. The weakened competition of the 2D charge order with superconductivity, as evinced by the lack of plateau in T_c and H_{c2}, is a consequence of disorder and inhomogeneity, which effectively smear out well defined transitions. Our measurements cannot discern whether Pr-YBCO hosts 3D charge order similar to YBCO, yet this is an interesting question for future work to disentangle its origin, if present, and its connection to crystal structure, 2D charge order and superconductivity.

ACKNOWLEDGMENTS

D.V. and C.P. acknowledges support from the EUR grant NanoX n°ANR-17-EURE-0009 and from the ANR grant NEPTUN n°ANR-19-CE30-0019-01. This work was supported by LNCMI-CNRS, members of the European Magnetic Field Laboratory (EMFL). Research at the University of California, San Diego, was supported by the US Department of Energy Basic Energy Sciences under Grant DE-FG02-04ER46105 (single crystal growth and characterization). A. F. acknowledges support from the National Science Foundation under Grant No. DMR-2145080.

Appendix A: Determination of T_c

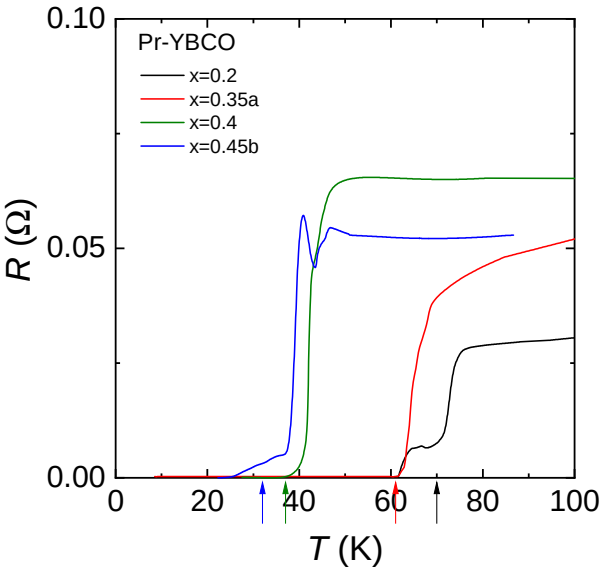

FIG. 7. Resistance versus temperature for four samples at nominal Pr content x=0.2, x=0.35, x=0.4, and x=0.45. T_c is defined as the temperature at which the transition extrapolates to $R = 0$. The exception is x=0.2 which shows a double transition in the resistivity. For this sample, we extrapolate the higher temperature transition to $R = 0$

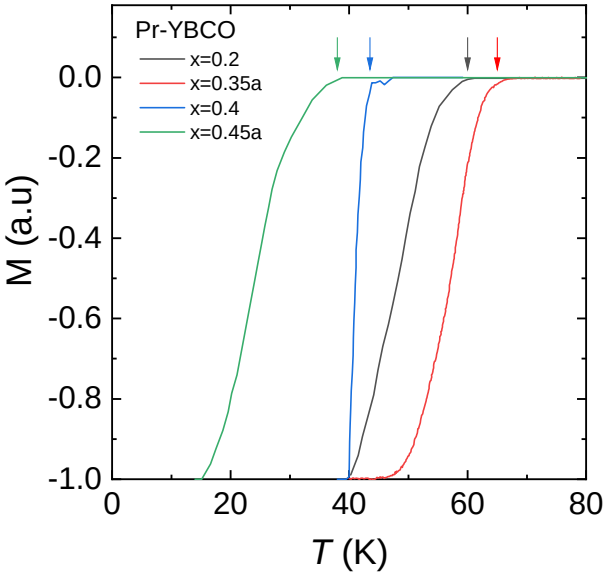

FIG. 8. Magnetization versus temperature for four samples at nominal Pr content x=0.2, x=0.35, x=0.4, and x=0.45. T_c is defined as the temperature at which magnetization start to decrease.

Appendix B: Sample dimensions

Sample	Nominal Pr x	Length (μm)	Width (μm)	Thickness (μm)
0.2	0.2	170	320	70
0.35a	0.35	290	590	100
0.35b	0.35	10	30	30
0.4	0.4	300	450	30
0.45a	0.45	220	190	50
0.45b	0.45	290	520	50

TABLE II. Dimensions of the samples measured in this work with their nominal Pr content.

Appendix C: Raw data

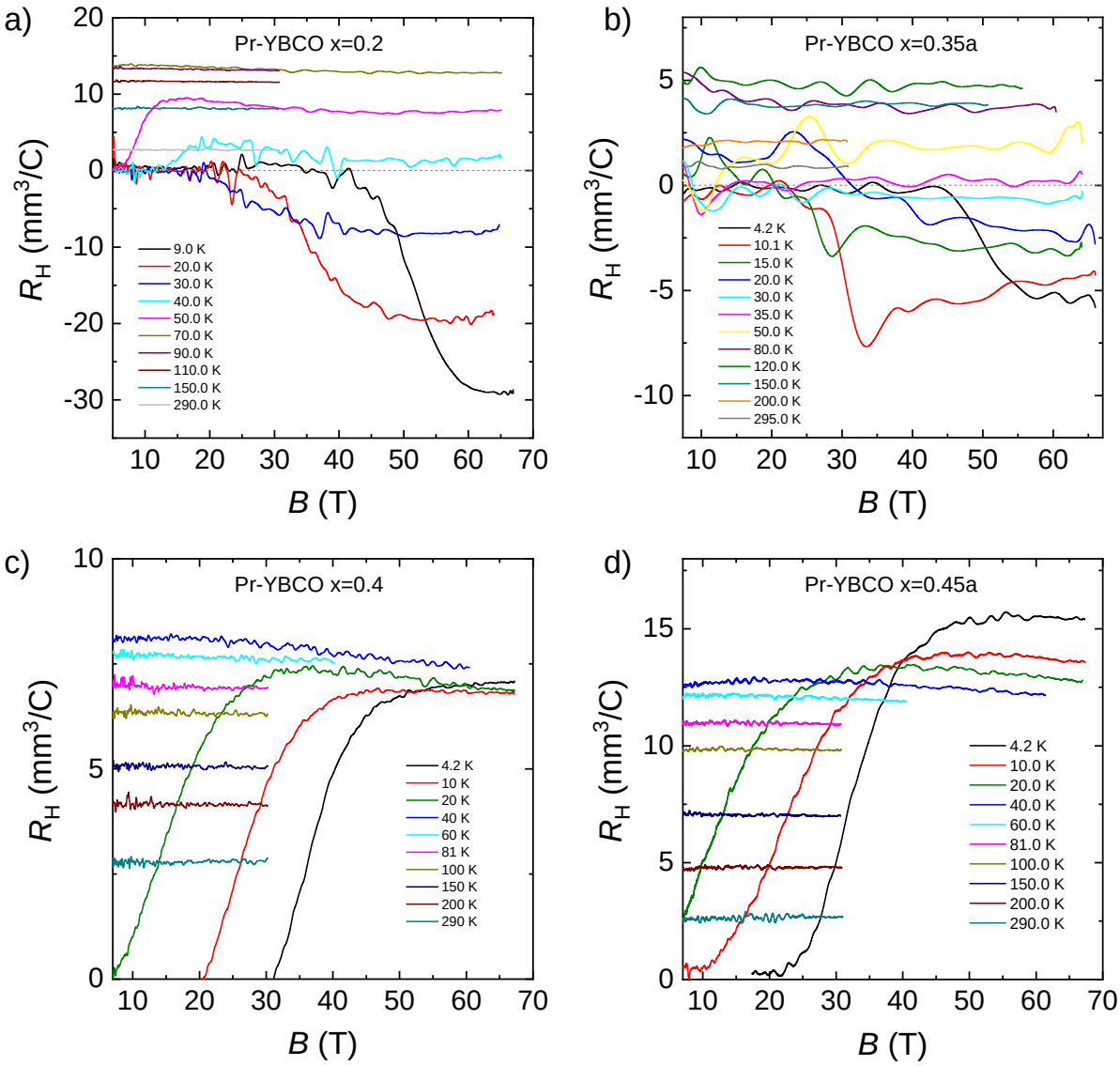

FIG. 9. R_H as a function of B at different temperatures for Pr-YBCO a) x=0.2, b) x=0.35, c) x=0.4, and d) x=0.45.

Appendix D: Reproductibility

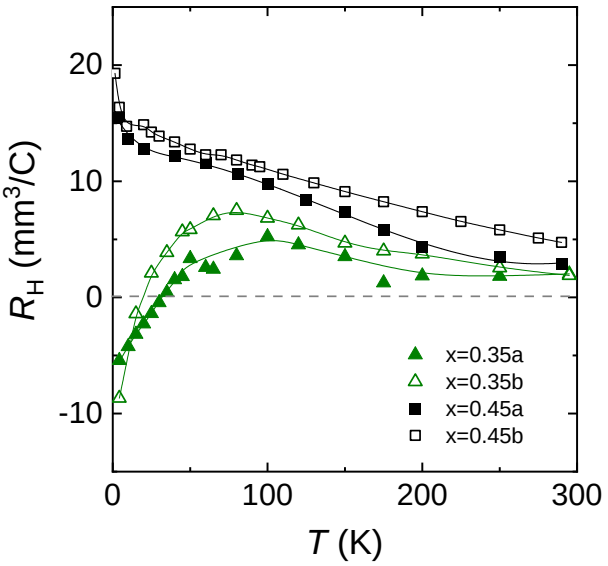

FIG. 10. $R_H(T)$ for two samples at nominal Pr content x=0.35 and two samples at x=0.45. Both samples at x=0.35 show a sign change of the Hall effect at low temperature, while $R_H(T)$ for both samples at x=0.45 remains positive down to low temperatures.

Appendix E: Determination of H_{c2}

In a strongly type-II superconductor with a high T_c the vortex lattice can melt at field values B_m well below H_{c2} for intermediate temperatures and assuming that the melting field B_m and $\mu_0 H_{c2}$ are equal at zero temperature, the melting transition field B_m is given by [65]

$$\frac{\sqrt{b_m(t)}}{1-b_m(t)}\frac{t}{\sqrt{1-t}}\left[\frac{4(\sqrt{2}-1)}{\sqrt{1-b_m(t)}}+1\right]=\frac{2\pi c_L^2}{\sqrt{G_i}} \qquad \text{(E1)}$$

The reduced field variable is $b_m = B_m/\mu_0 H_{c2}$, and $t = T/T_c$ is the reduced temperature. G_i is the Ginzburg number and c_L is the Lindemann number. Fig. 11 shows the vortex lattice melting transition for several Pr content. The dashed line are fit to Eq. E1 using c_L=0.2-0.3 and G_i=50.10^{-3} that give $\mu_0 H_{c2}$ displayed in Fig. 5.

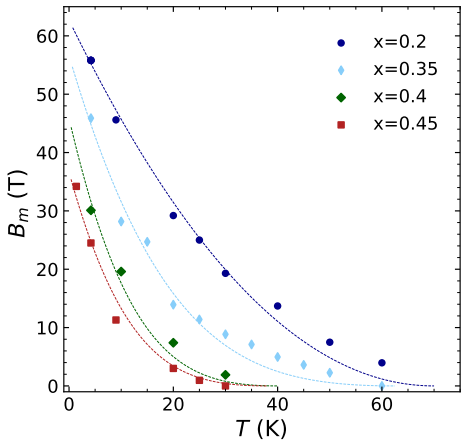

FIG. 11. Melting field B_m versus temperature for four samples at nominal Pr content x=0.2, x=0.35, x=0.4, and x=0.45. The dashed lines correspond to fit to Eq. E1.

Note that in ref. [52], the authors used a linear extrapolation from measurements up to 5 T over a temperature range of about 10 K near T_c for each doping level. Within this small temperature range, they remarked that the change in H_{c2}, namely d(H_{c2})/dT, is approximately linear and this linear extrapolation to $T = 0$ gives $H_{c2}(0)$. Therefore, the trend of the extrapolated $H_{c2}(0)$ versus doping can be trusted but the absolute values of $H_{c2}(0)$ have large error bars.

†caitlin.duffy@lncmi.cnrs.fr
‡cyril.proust@lncmi.cnrs.fr

[1] M. Akhavan, The question of Pr in HTSC, Physica B: Condensed Matter **321**, 265 (2002), proceedings of the Second Regional Conference on Magnetic and Superconducting Materials.
[2] M. B. Maple, C. C. Almasan, C. L. Seaman, S. H. Han, K. Yoshiara, M. Buchgeister, L. M. Paulius, B. W. Lee, D. A. Gajewski, R. F. Jardim, *et al.*, Extraordinary behaviour of the $Y_{1-x}Pr_xBa_2Cu_3O_{7-\delta}$ system, Journal of Superconductivity **7**, 97 (1994).
[3] H. B. Radousky, A review of the superconducting and normal state properties of $Y_{1-x}Pr_xBa_2Cu_3O_7$, Journal of Materials Research **7**, 1917 (1992).
[4] C. H. Booth, F. Bridges, J. B. Boyce, T. Claeson, Z. X. Zhao, and P. Cervantes, Local disorder in the oxygen environment around praseodymium in $Y_{1-x}Pr_xBa_2Cu_3O_7$ from x-ray-absorption fine structure, Phys. Rev. B **49**, 3432 (1994).
[5] J. Neumeier, T. Bjørnholm, M. Maple, J. Rhyne, and J. Gotaas, Neutron diffraction study of Pr valence and oxygen ordering in the $Y_{1-x}Pr_xBa_2Cu_3O_{7-\delta}$ system, Physica C: Superconductivity **166**, 191 (1990).
[6] R. Fehrenbacher and T. M. Rice, Unusual electronic structure of $PrBa_2Cu_3O_7$, Phys. Rev. Lett. **70**, 3471 (1993).
[7] J. Yang, Z. Jin, S. Wang, C. Moir, M. Xu, B. Gunn, X. Du, Z. Kang, K. Feng, M. Hashimoto, *et al.*, Superconductivity suppression and bilayer decoupling in Pr substituted $YBa_2Cu_3O_{7-\delta}$ (2025), arXiv:2510.15078 [cond-mat.supr-con].
[8] S. Badoux, W. Tabis, F. Laliberté, G. Grissonnanche, B. Vignolle, D. Vignolles, J. Béard, D. A. Bonn, W. N. Hardy, R. Liang, *et al.*, Change of carrier density at the

pseudogap critical point of a cuprate superconductor, Nature **531**, 210 (2016).

[9] D. W. Cooke, R. S. Kwok, R. L. Lichti, T. R. Adams, C. Boekema, W. K. Dawson, A. Kebede, J. Schwegler, J. E. Crow, and T. Mihalisin, Magnetic ordering in $(Y_{1-x}Pr_x)Ba_2Cu_3O_7$ as observed by muon-spin relaxation, Phys. Rev. B **41**, 4801 (1990).

[10] W. A. MacFarlane, J. Bobroff, P. Mendels, L. Cyrot, H. Alloul, N. Blanchard, G. Collin, and J.-F. Marucco, Planar ^{17}O NMR study of $Pr_yY_{1-y}Ba_2Cu_3O_{6+x}$, Phys. Rev. B **66**, 024508 (2002).

[11] D. Haug, V. Hinkov, Y. Sidis, P. Bourges, N. B. Christensen, A. Ivanov, T. Keller, C. T. Lin, and B. Keimer, Neutron scattering study of the magnetic phase diagram of underdoped $YBa_2Cu_3O_{6+x}$, New Journal of Physics **12**, 105006 (2010).

[12] M. Kang, C. C. Zhang, E. Schierle, S. McCoy, J. Li, R. Sutarto, A. Suter, T. Prokscha, Z. Salman, E. Weschke, *et al.*, Discovery of charge order in a cuprate Mott insulator, Proceedings of the National Academy of Sciences **120**, e2302099120 (2023).

[13] L. Martinelli, S. Rüdiger, I. Bialo, J. Oppliger, F. I. Saldana, M. v. Zimmermann, E. Weschke, R. Arpaia, and J. Chang, Differentiation of Site-Specific Symmetry Breaking Orders in $Y_{1-x}Pr_xBa_2Cu_3O_{6+y}$, (2025), arXiv:2507.20640.

[14] G. Ghiringhelli, M. L. Tacon, M. Minola, S. Blanco-Canosa, C. Mazzoli, N. B. Brookes, G. M. D. Luca, A. Frano, D. G. Hawthorn, F. He, *et al.*, Long-Range Incommensurate Charge Fluctuations in $(Y,Nd)Ba_2Cu_3O_{6+x}$, Science **337**, 821 (2012).

[15] J. Chang, E. Blackburn, A. T. Holmes, N. B. Christensen, J. Larsen, J. Mesot, R. Liang, D. A. Bonn, W. N. Hardy, A. Watenphul, *et al.*, Direct observation of competition between superconductivity and charge density wave order in $YBa_2Cu_3O_{6.67}$, Nature Physics **8**, 871 (2012).

[16] H.-H. Wu, M. Buchholz, C. Trabant, C. F. Chang, A. C. Komarek, F. Heigl, M. Zimmermann, M. Cwik, F. Nakamura, M. Braden, and C. Schüßler-Langeheine, Charge stripe order near the surface of 12-percent doped $La_{2-x}Sr_xCuO_4$, Nature Communications **3**, 1023 (2012).

[17] D. LeBoeuf, S. Krämer, W. N. Hardy, R. Liang, D. A. Bonn, and C. Proust, Thermodynamic phase diagram of static charge order in underdoped $YBa_2Cu_3O_y$, Nature Physics **9**, 79 (2013).

[18] R. Comin, A. Frano, M. M. Yee, Y. Yoshida, H. Eisaki, E. Schierle, E. Weschke, R. Sutarto, F. He, A. Soumyanarayanan, *et al.*, Charge Order Driven by Fermi-Arc Instability in $Bi_2Sr_{2-x}La_xCuO_{6+\delta}$, Science **343**, 390 (2014).

[19] W. Tabis, B. Yu, I. Bialo, M. Bluschke, T. Kolodziej, A. Kozlowski, E. Blackburn, K. Sen, E. M. Forgan, M. v. Zimmermann, *et al.*, Synchrotron x-ray scattering study of charge-density-wave order in $HgBa_2CuO_{4+\delta}$, Phys. Rev. B **96**, 134510 (2017).

[20] V. Oliviero, I. Gilmutdinov, D. Vignolles, S. Benhabib, N. Bruyant, A. Forget, D. Colson, W. A. Atkinson, and C. Proust, Charge order near the antiferromagnetic quantum critical point in the trilayer high Tc cuprate $HgBa_2Ca_2Cu_3O_{8+\delta}$, npj Quantum Materials **9**, 75 (2024).

[21] Q. Li, M. Hücker, G. D. Gu, A. M. Tsvelik, and J. M. Tranquada, Two-Dimensional Superconducting Fluctuations in Stripe-Ordered $La_{1.875}Ba_{0.125}CuO_4$, Phys. Rev. Lett. **99**, 067001 (2007).

[22] M. Fujita, H. Goka, K. Yamada, J. M. Tranquada, and L. P. Regnault, Stripe order, depinning, and fluctuations in $La_{1.875}Ba_{0.125}CuO_4$ and $La_{1.875}Ba_{0.075}Sr_{0.050}CuO_4$, Phys. Rev. B **70**, 104517 (2004).

[23] M. Frachet, I. Vinograd, R. Zhou, S. Benhabib, S. Wu, H. Mayaffre, S. Krämer, S. K. Ramakrishna, A. P. Reyes, J. Debray, *et al.*, Hidden magnetism at the pseudogap critical point of a cuprate superconductor, Nature Physics **16**, 1064 (2020).

[24] R. Liang, D. A. Bonn, and W. N. Hardy, Evaluation of CuO_2 plane hole doping in $YBa_2Cu_3O_{6+x}$ single crystals, Phys. Rev. B **73**, 180505 (2006).

[25] Y. Koike, N. Watanabe, T. Noji, and Y. Saito, Effects of the Cu-site substitution on the anomalous x dependence of T_c in $La_{2-x}Ba_xCuO_4$, Solid State Communications **78**, 511 (1991).

[26] J. L. Cohn, C. P. Popoviciu, Q. M. Lin, and C. W. Chu, Hole localization in underdoped superconducting cuprates near $\frac{1}{8}$ doping, Phys. Rev. B **59**, 3823 (1999).

[27] Z. Guguchia, B. Roessli, R. Khasanov, A. Amato, E. Pomjakushina, K. Conder, Y. J. Uemura, J. M. Tranquada, H. Keller, and A. Shengelaya, Complementary Response of Static Spin-Stripe Order and Superconductivity to Nonmagnetic Impurities in Cuprates, Phys. Rev. Lett. **119**, 087002 (2017).

[28] G. Grissonnanche, O. Cyr-Choinière, F. Laliberté, S. René de Cotret, A. Juneau-Fecteau, S. Dufour-Beauséjour, M.-È. Delage, D. LeBoeuf, J. Chang, B. J. Ramshaw, *et al.*, Direct measurement of the upper critical field in cuprate superconductors, Nature Communications **5**, 3280 (2014).

[29] O. Cyr-Choinière, D. LeBoeuf, S. Badoux, S. Dufour-Beauséjour, D. A. Bonn, W. N. Hardy, R. Liang, D. Graf, N. Doiron-Leyraud, and L. Taillefer, Sensitivity of T_c to pressure and magnetic field in the cuprate superconductor $YBa_2Cu_3O_y$: Evidence of charge-order suppression by pressure, Phys. Rev. B **98**, 064513 (2018).

[30] D. LeBoeuf, N. Doiron-Leyraud, B. Vignolle, M. Sutherland, B. J. Ramshaw, J. Levallois, R. Daou, F. Laliberté, O. Cyr-Choinière, J. Chang, *et al.*, Lifshitz critical point in the cuprate superconductor $YBa_2Cu_3O_y$ from high-field Hall effect measurements, Phys. Rev. B **83**, 054506 (2011).

[31] N. Doiron-Leyraud, S. Lepault, O. Cyr-Choiniere, B. Vignolle, G. Grissonnanche, F. Laliberté, J. Chang, N. Barišić, M. Chan, L. Ji, *et al.*, Hall, seebeck, and nernst coefficients of underdoped $HgBa_2CuO_{4+\delta}$: Fermi-surface reconstruction in an archetypal cuprate superconductor, Phys. Rev. X **3**, 021019 (2013).

[32] F. Laliberté, J. Chang, N. Doiron-Leyraud, E. Hassinger, R. Daou, M. Rondeau, B. J. Ramshaw, R. Liang, D. A. Bonn, W. N. Hardy, *et al.*, Fermi-surface reconstruction by stripe order in cuprate superconductors, Nature Communications **2**, 432 (2011).

[33] A. Gourgout, G. Grissonnanche, F. Laliberté, A. Ataei, L. Chen, S. Verret, J.-S. Zhou, J. Mravlje, A. Georges, N. Doiron-Leyraud, and L. Taillefer, Seebeck Coefficient in a Cuprate Superconductor: Particle-Hole Asymmetry in the Strange Metal Phase and Fermi Surface Transformation in the Pseudogap Phase, Phys. Rev. X **12**, 011037 (2022).

[34] R. Zhou, I. Vinograd, H. Mayaffre, J. Porras, H.-H.

Kim, T. Loew, Y. Liu, M. Le Tacon, B. Keimer, and M.-H. Julien, Robust Charge Density Wave Correlations in Optimally Doped $YBa_2Cu_3O_y$, Phys. Rev. Lett. **135**, 106503 (2025).

[35] N. Doiron-Leyraud, C. Proust, D. LeBoeuf, J. Levallois, J.-B. Bonnemaison, R. Liang, D. A. Bonn, W. N. Hardy, and L. Taillefer, Quantum oscillations and the Fermi surface in an underdoped high-Tc superconductor, Nature **447**, 565 (2007).

[36] E. A. Yelland, J. Singleton, C. H. Mielke, N. Harrison, F. F. Balakirev, B. Dabrowski, and J. R. Cooper, Quantum Oscillations in the Underdoped Cuprate $YBa_2Cu_4O_8$, Phys. Rev. Lett. **100**, 047003 (2008).

[37] A. F. Bangura, J. D. Fletcher, A. Carrington, J. Levallois, M. Nardone, B. Vignolle, P. J. Heard, N. Doiron-Leyraud, D. LeBoeuf, L. Taillefer, *et al.*, Small Fermi Surface Pockets in Underdoped High Temperature Superconductors: Observation of Shubnikov–de Haas Oscillations in $YBa_2Cu_4O_8$, Phys. Rev. Lett. **100**, 047004 (2008).

[38] N. Barišić, S. Badoux, M. K. Chan, C. Dorow, W. Tabis, B. Vignolle, G. Yu, J. Béard, X. Zhao, C. Proust, and M. Greven, Universal quantum oscillations in the underdoped cuprate superconductors, Nature Physics **9**, 761 (2013).

[39] M. K. Chan, N. Harrison, R. D. McDonald, B. J. Ramshaw, K. A. Modic, N. Barišić, and M. Greven, Single reconstructed fermi surface pocket in an underdoped single-layer cuprate superconductor, Nature Communications **7**, 12244 (2016).

[40] B. Vignolle, A. Carrington, R. A. Cooper, M. M. J. French, A. P. Mackenzie, C. Jaudet, D. Vignolles, C. Proust, and N. E. Hussey, Quantum oscillations in an overdoped high-Tc superconductor, Nature **455**, 952 (2008).

[41] N. Harrison and S. E. Sebastian, Fermi surface reconstruction from bilayer charge ordering in the underdoped high temperature superconductor $YBa_2Cu_3O_{6+x}$, New Journal of Physics **14**, 095023 (2012).

[42] S. Gerber, H. Jang, H. Nojiri, S. Matsuzawa, H. Yasumura, D. A. Bonn, R. Liang, W. N. Hardy, Z. Islam, A. Mehta, S. Song, *et al.*, Three-dimensional charge density wave order in $YBa_2Cu_3O_{6.67}$ at high magnetic fields, Science **350**, 949 (2015).

[43] J. Chang, E. Blackburn, O. Ivashko, A. T. Holmes, N. B. Christensen, M. Hücker, R. Liang, D. A. Bonn, W. N. Hardy, U. Rütt, *et al.*, Magnetic field controlled charge density wave coupling in underdoped $YBa_2Cu_3O_{6+x}$, Nature Communications **7**, 11494 (2016).

[44] H.-H. Kim, S. M. Souliou, M. E. Barber, E. Lefrançois, M. Minola, M. Tortora, R. Heid, N. Nandi, R. A. Borzi, G. Garbarino, *et al.*, Uniaxial pressure control of competing orders in a high-temperature superconductor, Science **362**, 1040 (2018).

[45] M. Bluschke, A. Frano, E. Schierle, D. Putzky, F. Ghorbani, R. Ortiz, H. Suzuki, G. Christiani, G. Logvenov, E. Weschke, *et al.*, Stabilization of three-dimensional charge order in $YBa_2Cu_3O_{6+x}$ via epitaxial growth, Nature Communications **9**, 2978 (2018).

[46] H. Jang, W.-S. Lee, H. Nojiri, S. Matsuzawa, H. Yasumura, L. Nie, A. V. Maharaj, S. Gerber, Y.-J. Liu, A. Mehta, *et al.*, Ideal charge-density-wave order in the high-field state of superconducting YBCO, Proceedings of the National Academy of Sciences **113**, 14645 (2016).

[47] A. Ruiz, B. Gunn, Y. Lu, K. Sasmal, C. M. Moir, R. Basak, H. Huang, J.-S. Lee, F. Rodolakis, T. J. Boyle, *et al.*, Stabilization of three-dimensional charge order through interplanar orbital hybridization in $Pr_xY_{1-x}Ba_2Cu_3O_{6+\delta}$, Nature Communications **13**, 6197 (2022).

[48] I. Vinograd, S. M. Souliou, A.-A. Haghighirad, T. Lacmann, Y. Caplan, M. Frachet, M. Merz, G. Garbarino, Y. Liu, S. Nakata, *et al.*, Using strain to uncover the interplay between two- and three-dimensional charge density waves in high-temperature superconducting $YBa_2Cu_3O_y$, Nature Communications **15**, 3277 (2024).

[49] S. Blanco-Canosa, A. Frano, E. Schierle, J. Porras, T. Loew, M. Minola, M. Bluschke, E. Weschke, B. Keimer, and M. Le Tacon, Resonant x-ray scattering study of charge-density wave correlations in $YBa_2Cu_3O_{6+x}$, Phys. Rev. B **90**, 054513 (2014).

[50] L. Paulius, B. Lee, M. Maple, and P. Tsai, Preparation and characterization of $Y_{1-x}Pr_xBa_2Cu_3O_{7-\delta}$ single crystals, Physica C: Superconductivity **230**, 255 (1994).

[51] S. Kunisada, S. Isono, Y. Kohama, S. Sakai, C. Bareille, S. Sakuragi, R. Noguchi, K. Kurokawa, K. Kuroda, Y. Ishida, S. Adachi, R. Sekine, T. K. Kim, C. Cacho, S. Shin, T. Tohyama, K. Tokiwa, and T. Kondo, Observation of small Fermi pockets protected by clean CuO_2 sheets of a high-T_c superconductor, Science **369**, 833 (2020).

[52] Y. X. Jia, J. Z. Liu, M. D. Lan, P. Klavins, R. N. Shelton, and H. B. Radousky, Upper critical field H_{c2} of single-crystal $Y_{1-x}Pr_xBa_2Cu_3O_{7-\delta}$, Phys. Rev. B **45**, 10609 (1992).

[53] F. Laliberté, M. Frachet, S. Benhabib, B. Borgnic, T. Loew, J. Porras, M. Le Tacon, B. Keimer, S. Wiedmann, C. Proust, and D. LeBoeuf, High field charge order across the phase diagram of $YBa_2Cu_3O_y$, npj Quantum Materials **3**, 11 (2018).

[54] Y. Gannot, B. J. Ramshaw, and S. A. Kivelson, Fermi surface reconstruction by a charge density wave with finite correlation length, Phys. Rev. B **100**, 045128 (2019).

[55] H. Yao, D.-H. Lee, and S. Kivelson, Fermi-surface reconstruction in a smectic phase of a high-temperature superconductor, Phys. Rev. B **84**, 012507 (2011).

[56] S. Nakata, P. Yang, M. E. Barber, K. Ishida, H.-H. Kim, T. Loew, M. Le Tacon, A. P. Mackenzie, M. Minola, C. W. Hicks, and B. Keimer, Normal-state charge transport in $YBa_2Cu_3O_{6.67}$ under uniaxial stress, npj Quantum Materials **7**, 118 (2022).

[57] L. Nie, G. Tarjus, and S. A. Kivelson, Quenched disorder and vestigial nematicity in the pseudogap regime of the cuprates, Proceedings of the National Academy of Sciences **111**, 7980 (2014).

[58] J. A. W. Straquadine, F. Weber, S. Rosenkranz, A. H. Said, and I. R. Fisher, Suppression of charge density wave order by disorder in Pd-intercalated $ErTe_3$, Phys. Rev. B **99**, 235138 (2019).

[59] S. Blanco-Canosa, A. Frano, T. Loew, Y. Lu, J. Porras, G. Ghiringhelli, M. Minola, C. Mazzoli, L. Braicovich, E. Schierle, *et al.*, Momentum-Dependent Charge Correlations in $YBa_2Cu_3O_{6+\delta}$ Superconductors Probed by Resonant X-Ray Scattering: Evidence for Three Competing Phases, Phys. Rev. Lett. **110**, 187001 (2013).

[60] P. Abrami, *Magnetic Torque and Transport Investigation of the Pseudogap and CDW in* $YBa_2Cu_3O_{6-x}$, Ph.D. the-

sis, University of Bristol (2021).
[61] M. Hücker, N. B. Christensen, A. T. Holmes, E. Blackburn, E. M. Forgan, R. Liang, D. A. Bonn, W. N. Hardy, O. Gutowski, M. v. Zimmermann, *et al.*, Competing charge, spin, and superconducting orders in underdoped $YBa_2Cu_3O_y$, Phys. Rev. B **90**, 054514 (2014).
[62] J. L. Tallon, C. Bernhard, G. V. M. Williams, and J. W. Loram, Zn-induced T_c reduction in high- T_c superconductors: Scattering in the presence of a pseudogap, Phys. Rev. Lett. **79**, 5294 (1997).
[63] A. Yamamoto, W.-Z. Hu, and S. Tajima, Thermoelectric power and resistivity of $HgBa_2CuO_{4+\delta}$ over a wide doping range, Phys. Rev. B **63**, 024504 (2000).
[64] J. Neumeier, M. Maple, and M. Torikachvili, Pressure dependence of the superconducting transition temperature of $(Y_{1-x}Pr_x)Ba_2Cu_3O_{7-\delta}$ compounds; Evidence for 4f electron hybridization, Physica C: Superconductivity **156**, 574 (1988).
[65] G. Blatter, M. V. Feigel'man, V. B. Geshkenbein, A. I. Larkin, and V. M. Vinokur, Vortices in high-temperature superconductors, Rev. Mod. Phys. **66**, 1125 (1994).